Chapter 4

Adsorption using Composite

4.1 Removal of Cu^{2+} , Ni^{2+} and Zn^{2+} ions by Composite

Bentonite is an anionic soft and fine clay, which has incredible ability of heavy metal binding. Extraordinary surface area and loftier Fe/Mn/aluminium oxide content also complements the adsorption efficiency of bentonite [236]. Enhancement in the metal uptake capacity of soil after addition of bentonite was reported by Kumararaja et al., 2014 [237]. Akpomie and Dawodu (2015) discovered a remarkable change in adsorption capacity as well as a strong regeneration ability (90%) in Nigerian bentonite for nickel and manganese removal [238]. Additionally, inorganic coagulants were blended with bentonite clay for scavenging heavy metal ions from acid mine drainage [239]. A phenomenon of complex formation and ion-exchange mechanism was reported during adsorption of lead, cadmium, mercury and chromium on the surface of low-cost silk fibroin-based bentonite composite [240]. Wahab et al., 2019 [240] conveyed that addition of silk fibroin increased the adsorption capacity of the composite. The surface of red mud is mesoporous and has enormous potential for adsorbing copper, lead and chromium ions from the aqueous phase [241]. Shin et al., 2014 [242] performed multi-metal adsorption and found that red mud had higher uptake capacity as compared to oyster shell, zeolite and limestone. The higher adsorption of heavy metals in their study was due to the presence of the Si-Al-O bond in red mud [242]. The composite made up of red mud and polyacrylic acid showed higher

sorption capacity (96.15 mg/g) for cadmium than red mud (21.7 mg/g) [170].

The modeling of adsorption is a critical step prior to implementing strategies in the industrial pollution abetment. Models are designed, developed, tested and optimized using several techniques like ANN, genetic algorithm, simulated annealing, first principle and population balance. Among these techniques, ANN has attracted courtesy of researchers due to its ease of use, accuracy and model robustness [233].

Jaskulak et al., 2020 [243] used ANN to predict the heavy metal removal from the contaminated soil. The ANN models were used by the authors to predict and compare output function with experimental results through regression coefficient and model efficiency equations. Jaskulak et al., 2020 [243] reported high coefficient of determination (R = 0.9983) and lowest root mean square errors, MSE (0.31). Mohammadi et al., 2019 [244] carried out pyrene removal from the soil by phytoremediation and modeled using RSM and ANN. Mohammadi et al., 2019 [244] found that the predictability approach of ANN was better than RSM based on higher R and lowest MSE. The molecular dynamics of adsorption is principally represented through estimation of dimensionless numbers. This is very supportive in the selection of adsorbent, design and development, scale-up and fabrication continuous adsorption reactors including pressure swing adsorbers. Adsorption dynamics of adsorption is very scarcely reported in the scientific literature. The authors [245], [246] utilized transfer kinetic equation based on SRT to develop molecular dynamics of adsorption at solid-liquid interphase.

The objective of this study was to develop a novel composite made of bentonite clay and red ochre that can act as an efficient scavenger of Cu^{2+}, Ni^{2+} and Zn^{2+} in the liquid phase. Further, to select the scale-up criterion and reactor configuration for composite mediated reactors, Adsorption dynamics and predictive modeling through ANN of Cu^{2+}, Ni^{2+} and Zn^{2+} over the composite surface was done. Additionally, physicochemical characterization of the composite was done through FTIR, SEM, zero-point charge (pH_{zpc}), BET surface area, ultimate analysis and XRD. Isotherm, kinetic and thermodynamic modeling of the experimental data was done to explore the nature of adsorption and uptake capacity of the composite.

Finally, to demonstrate the composite's applicability, we conducted not only a comparative study with other adsorbents but also attempted to adhere to the standards for the permitted level of Cu^{2+}, Ni^{2+} and Zn^{2+} ions discharge as prescribed by USEPA, WHO, BIS, CPCB and ICMR.

4.2 Results and discussion

4.2.1 Physicochemical characterization

4.2.1.1 SEM

The SEM of the composite before and after adsorption are shown in Figures 4.1a and 4.1b.

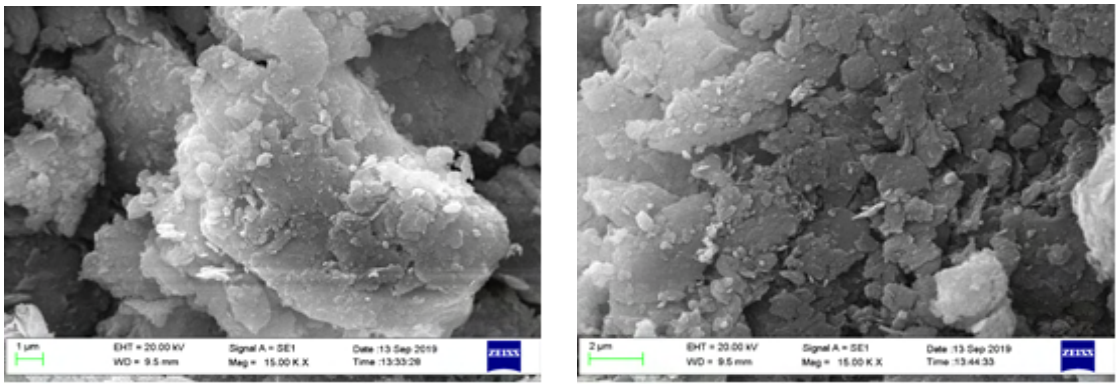

(a) Before adsorption **(b)** After adsorption

Figure 4.1: SEM of composite before and after adsorption of ternary metal ions

Figure 4.1a showed small particles consisting of platelets conglomerated with the larger particles. At 15 kX magnification, the cavities were visible on the surface of composite. The fluffy layered sheet structure transformed into the rugged and foliated layered structure after adsorption (Figure 4.1b) [247]–[249]. Ogunmodede et al., 2015 [250] observed platelets of bentonite clusters in larger particles. Additionally, Bilal et al., 2016 [251] reported dispersed structures in bentonite due to the presence of randomly shaped alumina. Similar to the present study, another group of researchers Dodoo-Arhin et al., 2017 [252] analyzed red mud-cement based composites and found particles with plate-like shapes and agglomerates in the SEM micrograph. The EDX of the composite has been shown in Figure 4.2 and 4.3. Peaks of Na, Mg, Ca, Al and Fe in composite were due to the

inherent characteristics of bentonite clay and red ochre. Figure 4.2 showed the absence

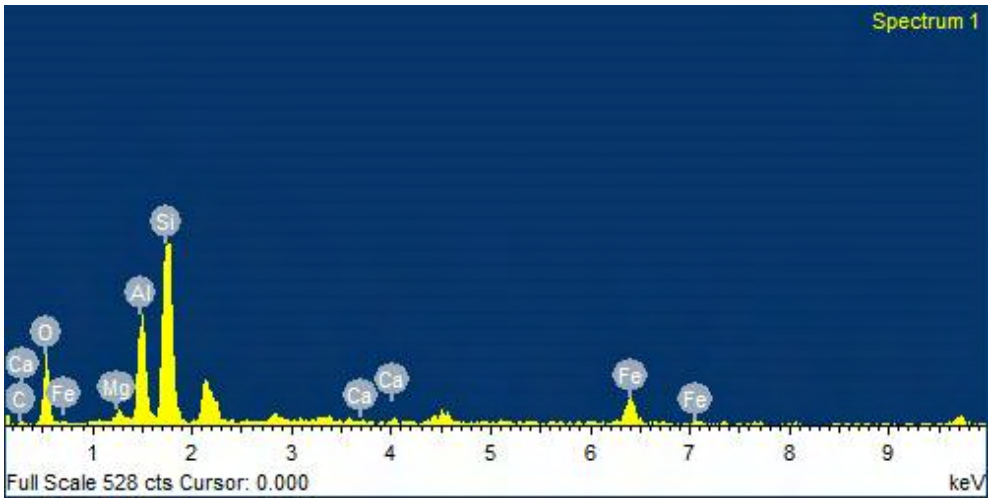

Figure 4.2: EDX of composite before adsorption of ternary metal ions

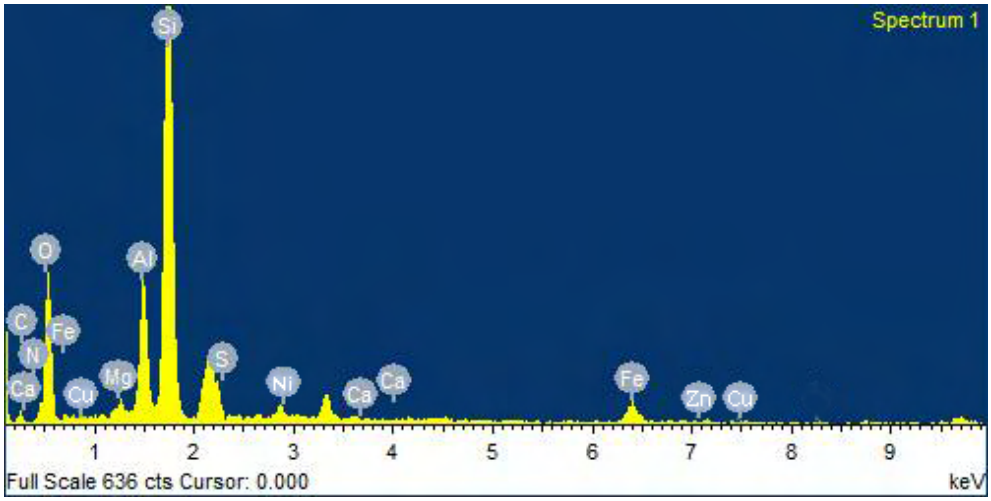

Figure 4.3: EDX of composite after adsorption of ternary metal ions

of Cu^{2+}, Ni^{2+} and Zn^{2+} ions on the surface of composite before adsorption. However, after adsorption, significant amount of Cu^{2+}, Ni^{2+} and Zn^{2+} ions were observed from Figure 4.3.

4.2.1.2 FTIR

The FTIR of the composite is shown in Figure 4.4.

The bands around 3700 cm^{-1} were due to hydroxyl group in di-octahedral part of the mineral each pair of Al^{3+} ions have two OH groups which are related by centre of symmetry between Al^{3+}.

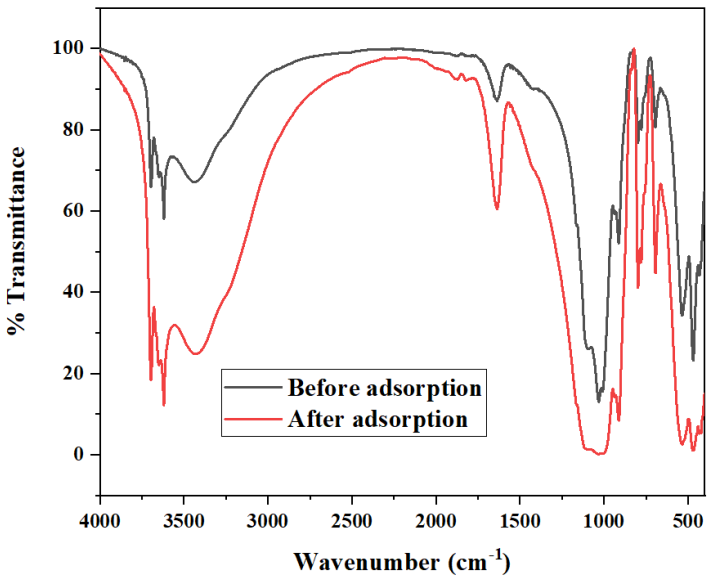

Figure 4.4: FTIR of composite before and after adsorption of ternary metal ions

Peaks at 3444.32 and 3430.37 cm^{-1} were attributed to the hydration stretching of the hydroxyl group due to the presence of Al-AlOH and Al-MgOH in the aluminium rich octahedral centers of bentonite. Likewise, Ravindra et al., 2017 [253] observed similar peaks at 3445 cm^{-1} during spectroscopic characterization of bentonite, which are attributed to the presence of structural hydroxyl groups in the material. Here, peaks at 1645.96 and 1641.86 cm^{-1} were due to deformation of water molecules [254]. Similar peaks were found by Castaldi et al., 2008 [255] during FTIR analysis of bauxite ore processing waste i.e., red mud at 1630 cm^{-1} that was attributed to the water molecules occluded inside the aluminosilicate structure. The bending vibration of the H-O-H group and Si-O bond stretching were observed at 1034.47 cm^{-1} and 1027.90 cm^{-1}, respectively. Similar to the peaks found in present study, Ravindra et al., 2017 [253] confirmed that the two components of maximum absorption sharp band near 1000 cm^{-1} (marked with black color in Figure 4.4) are a property of layered silicate montmorillonite mineral. Peaks at 798.08 cm^{-1} and 702.05 cm^{-1} were due to Si-O stretching of silica and quartz [256]. Si-O-Al bending was observed at 693.84 cm^{-1} which is similar to the results of [257]. Two prominent bands at 542.81 and 532.14 cm^{-1} were ascribed to hematite of ochre [258]. Castaldi et al., 2008 [255] observed similar peaks in spectra of red mud at 460-500 cm^{-1} and determined that the peak was caused by stretching vibrations of the Fe-O bond. The

transmittance peaks were observed at 3624, 3400, 1730, 1370, 789 and 696 cm^{-1} [256] which were also confirmed in the present study.In the FTIRs of composite before and after adsorption, there was change in the peaks (3444.32 to 3430.37cm^{-1}, 1645.96 to1641.86 cm^{-1}, 1034.47 cm^{-1} to 1027.90 cm^{-1}, 798.08 cm^{-1} to 702.05 cm^{-1}). This significant shift of wave numbers showed that adsorption of metals ions with the surface of the composite was mediated by chemisorption.

4.2.1.3 XRD

As depicted in Figure 4.5, an XRD analysis of the composite before and after the adsorption of ternary metal ions was performed. It is evident that after adsorption of Cu^{2+},

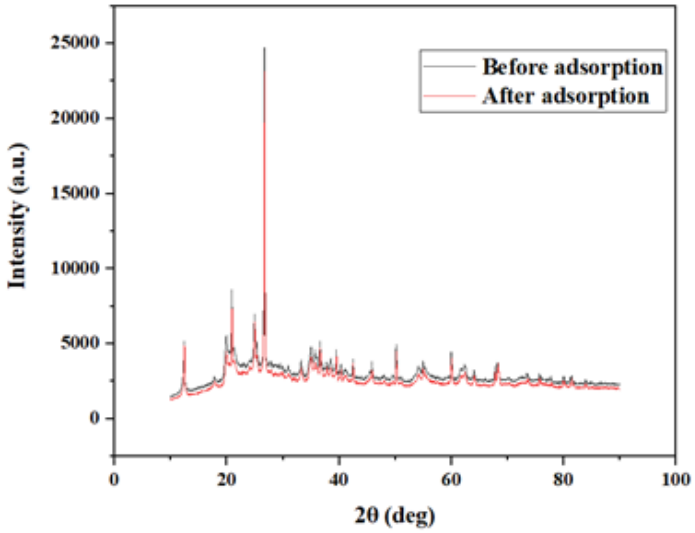

Figure 4.5: XRD of composite before and after adsorption of ternary metal ions

Ni^{2+} and Zn^{2+} ions, the intensity of peaks decreased. This demonstrated that metal ion adsorption on the composite surface caused the crystallinity of the composite to diminish. A reduction in crystallinity was observed during the adsorption of phosphate ions on the surface of red soil [259]. In the present work, peak positions before and after the adsorption remained the same, and the peaks at 2 θ (19.99° and 68.37°) were attributed to montmorillonite. Peaks at 20.84°, 33.44°, 39.46°, 45.76° and 54.99° showed quartz in the composite. Alumina was reported at 35.13°, 36.73° and 50.09° in the composite. The incidence of hematite was guaranteed at peaks 25.03°, 42.74° and 62.40°. The results of the

FTIR were in agreement with the results of XRD. Quartz, alumina and montmorillonite occur naturally in bentonite clay and hematite is a major component of red ochre [260]–[262]. XRD showed iron (hematite (Fe_2O_3)) in the ceramic pigments [261]. Similarly, Roman et al., 2015 [263] observed peaks of the hematite near to 42° and 62° and Rotondo et al., 2010 [260] characterized fifty different kinds of pigments through XRD and recorded peaks of Fe_2O_3 at 42º, 63º and 84º. Similarly, some of the authors like Rotondo et al., 2010 [260] and Bugoi et al., 2008 [261] also at witnessed peaks at 20°, 34° and 48° which were attributed to quartz in pigments. The findings of authors were in agreement with results obtained in the present study. Additionally, Fil et al., 2014 [262] characterized montmorillonite and divulged its dioctahedral structure through XRD peak near to 68° and also, Dankova et al., 2010 [264] found diffractogram peaks near to 20° and 68°, which confirmed the presence of montmorillonite in the composite.

4.2.1.4 BET Surface Area

The BET surface area of bentonite, red ochre and composite was found to be 197.04 m^2/g, 82.96 m^2/g and 447.31 m^2/g, respectively. Larger surface area of composite compared to pure bentonite was due to addition of red ochre. The BET surface area of bentonite clay was recorded as 43.48 m^2/g that was collected from the South Africa after removing fluoride from the aqueous solution [265]. Similarly, the BET surface area of red mud was found to be 32.77 m^2/g during adsorption cadmium from wastewater [266].

4.2.1.5 Ultimate Analysis

The result of ultimate analysis indicated 39.03 % carbon, 14.46 % nitrogen, 1.48 % hydrogen and 0% sulphur in the composite. These results showed the existence of organic matter within the composite (high carbon content). These findings enhanced the composite application as an metal ion scavenger for heavy metal ions [267]. Raghavendra et al., 2015 [268] observed the absence of nitrogen and sulphur in bentonite. Lower nitrogen and sulphur content in the samples suggests reduced emissions of NOx and SOx gases to the atmosphere during incineration of composite after adsorption [269]. This reflected that

the composite developed in this study was eco-friendly.

4.2.2 pH_{ZPC}

The pH_{zpc} of the composite was found to be 5.2 (Figure 4.6). At pH values higher than this, the surface of the composite is negatively charged, which aids in the removal of cations from the solution.

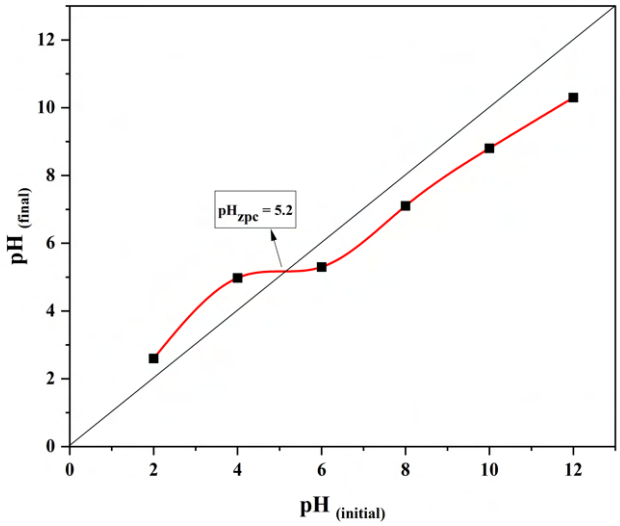

Figure 4.6: pH_{zpc} of composite

Similar results were observed during adsorption of lead and p-nitrophenol on the bentonite clay [270]. Naga et al., 2019 [271] found 6.7 pH_{zpc} during adsorption of As (III) on activated red mud doped calcium-alginate beads.

4.2.3 Adsorption Dynamics

In the present work, values of the film and pore diffusivity coefficients showed that adsorption is dependent upon film diffusion as the values lies between 10^{-6} to 10^{-8} for Zn^{2+}, Ni^{2+} and Cu^{2+} ions (Table 4.1).

The value of N_k was observed between 10^1 and 10^4 for Cu^{2+} and Ni^{2+} which elucidated that adsorption was controlled by diffusion and for Zn^{2+}, the process was mixed diffusion and transfer controlled as value lies between 10^{-3} and 10^1. The value of φ and λ were in

Table 4.1: Dimensionless numbers and diffusivity coefficients for composite

Dimensionless Number	φ	λ	N_k	D_p ($cm^2\ sec^{-1}$)	D_F ($cm^2\ sec^{-1}$)
Cu^{2+}	66.49	9.12×10^{-5}	38.63	4.03×10^{-10}	4.80×10^{-7}
Ni^{2+}	66.10	1.48×10^{-3}	38.86	2.83×10^{-10}	1.41×10^{-6}
Zn^{2+}	65.70	2.06×10^{-4}	3.91	1.75×10^{-10}	8.59×10^{-6}

the range of 10^{-2} to 10^{4} and 10^{-12} to 10^{8}, which showed thorough coverage of composite surface during adsorption with trim downed surface tension [213], [272].

4.2.4 ANN Modelling

pH, contact time, composite dose, temperature and adsorbate concentration were provided as network inputs. The back-propagation technique with the L-M algorithm was used to

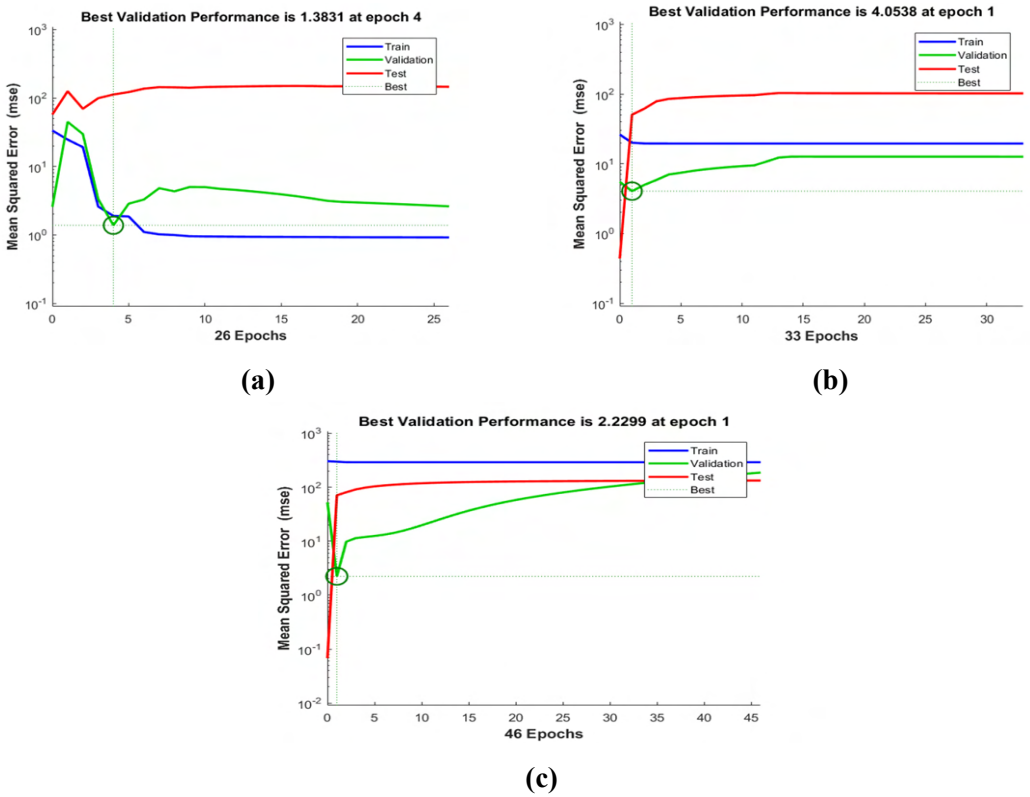

Figure 4.7: Performance between number of epochs and MSE for prediction of (a) Cu^{2+}, (b) Ni^{2+} and (c) Zn^{2+} ions removal using composite as adsorbent

predict output function. The network was trained until lesser number of epochs were obtained [235]. Thereafter, the network simulation was processed with the experimental

data. The predictive output function was compared with the experimental results. Figure 4.7 shows the MSE of the ANN model obtained in training, testing and validation of data. The lowest MSE (encircled point) was recorded during training, testing and validation of data by L-M algorithm. Similar results were found by Yildiz, 2018 [232] with best validation performance 0.0011846 at epochs 27 for Ni^{2+} ions.

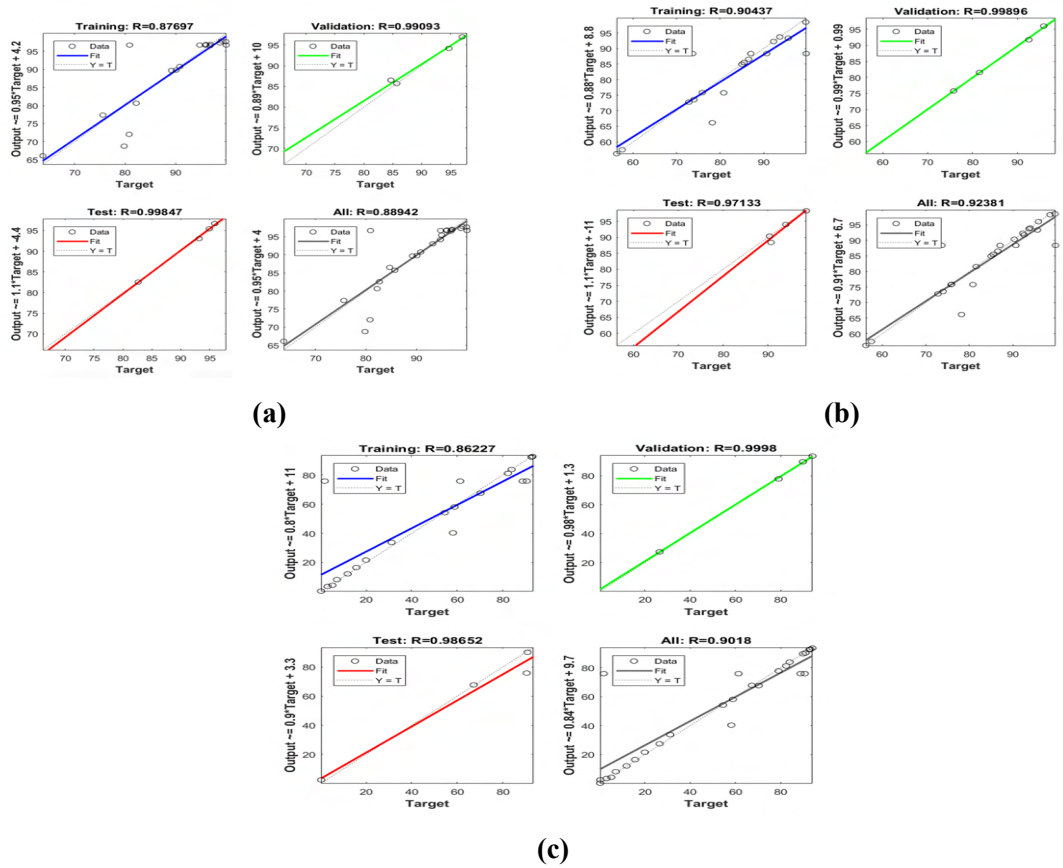

Figure 4.8: Regression plot for prediction of (a) Cu^{2+}, (b) Ni^{2+} and (c) Zn^{2+} ions removal using composite as adsorbent

Figure 4.8 shows regression between experimental and predicted values for the adsorption of ternary metal ions on composite. The circles in the plot are experimental values and the colored lines show the predicted values derived from ANN models. Both the experimental and theoretical values seemed to be in agreement with each other showing a high regression coefficient (R^2 value in range of 0.89 - 0.92). Thus, in the present work, the L-M algorithm was concluded appropriate for predicting the output function with the lowest MSE at epoch (4, 1, 1 for Cu^{2+}, Ni^{2+} and Zn^{2+} ions) coupled and highest validation performance in ten neurons at 1.3831, 4.0538 and 2.2299 for Cu^{2+}, Ni^{2+} and Zn^{2+}

ions, respectively (Figure 4.7). The results also showed a small deviation of 0.08% for

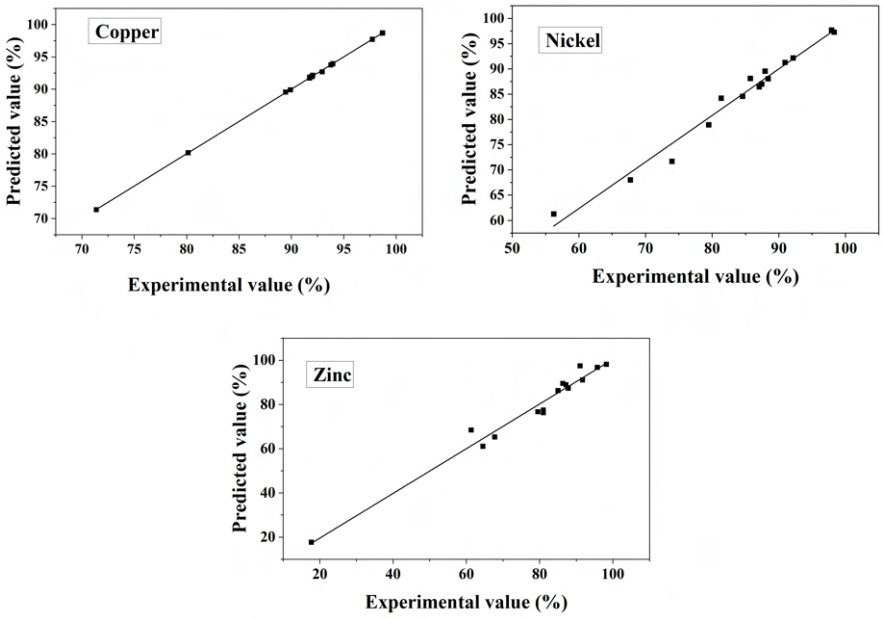

Figure 4.9: Correlation plot for the experimental and ANN predicted values for ternary metal ions removal using composite as adsorbent

Cu^{2+}, 1.26% for Ni^{2+} and 0.53% for Zn^{2+} ions between the experimental and predicted values (Figure 4.9). This further showed the suitability of L-M algorithm in the present work. ANN were also used for modeling Cu^{2+} adsorption on zeolite surface [273]. Adsorbent dose, contact time and pH were given as input for simulating experimental results. The authors observed that the L-M back-propagation training function with six neurons in the hidden layer were the most efficient network, similar to the present study. Similarly, Yildiz, 2018 [274] applied ANN in the adsorption of Ni^{2+} from aqueous solution on peanut shell surface and found a high regression coefficient ((R) training (0.99), test (0.97) and validation (0.99) between experimental and predicted values.

4.2.5 Adsorption Kinetics

The results of kinetics are shown in Figure 4.10 and Table 4.2.

It is evident from Figure 4.10 and Table 4.2 that the adsorption of ternary metal ions on the composite was best defined by the PSO model with lower value of SSR as compared to

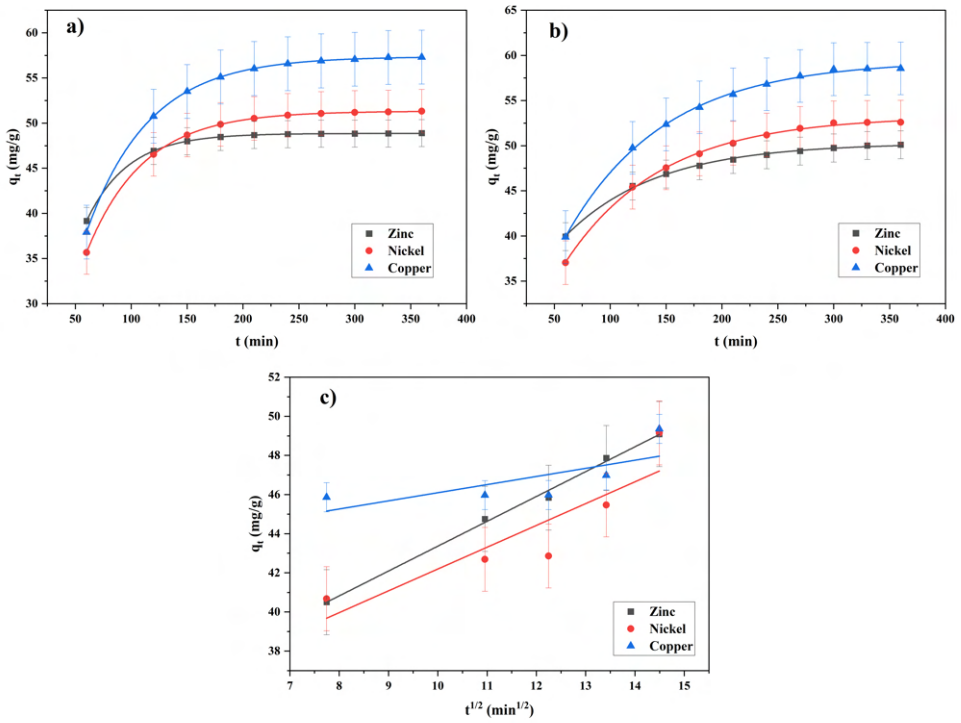

Figure 4.10: a) PFO **b)** PSO and **c)** IPD kinetic models for composite as adsorbent

Table 4.2: Adsorption kinetic model parameters for composite as adsorbent

Kinetic Parameter		PFO		PSO		IPD	
		q_e (mg/g)	k_1 min^{-1}	q_e (mg/g)	k_2 (g/mg. min)	k_p (mg/g. min)	C (mg/g)
Value	Cu^{2+}	9.46	0.032	10.50	0.004	0.29	5.36
	Ni^{2+}	9.46	0.027	10.69	0.003	0.33	4.67
	Zn^{2+}	9.65	0.017	11.28	0.002	0.38	3.44
SSR	Cu^{2+}	2.45		0.69		311.84	
	Ni^{2+}	2.63		0.88		127.13	
	Zn^{2+}	1.49		0.43		21.97	

the PFO and IPD model, this showed that the adsorption was mediated by chemisorption. These results complemented the findings of FTIR and XRD. Similar results were provided by Ghomri et al., 2013 [275] in adsorption of Cu^{2+}, Ni^{2+} and Zn^{2+} ions on natural bentonite. Mohellebi and Lakel, 2016 [276] testified that adsorption of Zn^{2+} onto untreated Algerian bentonite was mediated by chemisorptive mode. Similarly, Burham and Sayed, 2016 [267] communicated that the PSO model best fitted during adsorption of Zn^{2+} ions

onto sodium bentonite.

4.2.6 Adsorption Isotherm

Results of isotherm modeling are shown in Figure 4.11 and Table 4.3.

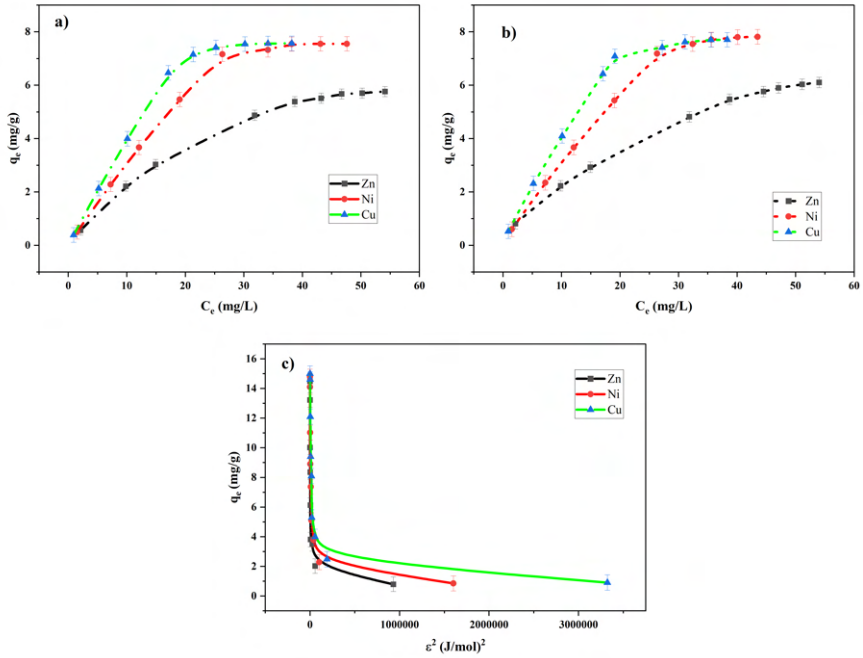

Figure 4.11: a) Langmuir **b)** Freundlich and **c)** D-R isotherms for composite as adsorbent

Table 4.3: Adsorption isotherm model parameters for composite as adsorbent

Isotherm		**Langmuir**		**Freundlich**		**D-R**	
Parameter		**q_m (mg/g)**	**K_L (L/mg)**	**n**	**K_F L/mg**	**E (kJ/mol)**	**q_e (mg/g)**
Value	**Cu^{2+}**	61.86	0.007	1.16	0.56	37.06	84.20
	Ni^{2+}	37.89	0.008	1.15	0.42	31.31	69.92
	Zn^{2+}	10.48	0.03	1.52	0.49	14.11	43.30
SSR	**Cu^{2+}**	2.64		4.47		123.70	
	Ni^{2+}	0.32		1.22		43.38	
	Zn^{2+}	1.99		2.83		199.78	

The results were best fitted to Langmuir isotherm in terms of lowest SSR for adsorption of all the metal ions as compared to other isotherms. The value of R_L was < 1 (0.58 for

Cu^{2+}, 0.55 for Ni^{2+} and 0.25 for Zn^{2+}) which depicted favorable adsorption [277]. In D-R isotherm, the value of 'E' was > 8 kJ/mol establishing the role of chemical adsorption on the surface of composite [278]. In Freundlich isotherm, 'n' was > 1 which indicated towards favorable adsorption [279]. Similar results were verified by researchers [280] during adsorption of Cu^{2+}, Ni^{2+} and Zn^{2+} ions on Chitosan-8-Hydroxyquinoline beads. A study conducted by Liu and Zhou, 2010 [224] investigated the adsorption of $Cu^{2+}$and Zn^{2+} on sodium bentonite and discovered that the Langmuir isotherm provided a better fit to the experimental data. In the same way, Sdiri et al., 2014 [281] showed the supremacy of Langmuir isotherm in the adsorption of Cu^{2+}, Ni^{2+} and Zn^{2} in single and binary metal ion systems.

Multi-metal systems function in the same way with copper as the most efficient adsorbate and zinc as the least. Cu^{2+} ions (2) have the highest electronegativity of all ions, implying stronger bond to functional groups. The second most adsorbed metal is Ni^{2+} ions (1.91) which also has the second highest electronegativity, followed by Zn^{2+} ions (1). This indicates that the adsorption of Cu^{2+}, Ni^{2+} and Zn^{2+} ions on composite material followed the same trend as electronegativity, i.e., Cu^{2+}> Ni^{2+}> Zn^{2+}. The adsorption capacity pattern of the mentioned ions has been shown in Table 4.3. This trend is the same in the research study conducted by Kemik et al., 2017 [282] during the removal of Cu^{2+}, Ni^{2+} and Zn^{2+} ions by using hydrogels.

4.2.7 Thermodynamics

Results of thermodynamic modeling are shown in Figure 4.12 and Table 4.4.

The value of ΔG was negative and decreased with the rise in temperature from 288 to 308 K which pointed towards the feasible and spontaneous adsorption of ternary metal ions at higher temperatures [274]. Furthermore, the value of ΔG was < 20 kJ/mol (Table 4.4) which showed the possibilities of electrostatic interaction between active sites of composite and Cu^{2+}, Ni^{2+} and Zn^{2+} ions [283]. The positive value of ΔH suggested the endothermic adsorption [284]. The positive ΔH can be explained by the fact that the metal ion hydration sphere is destroyed before the metal ion adsorption took place on the com-

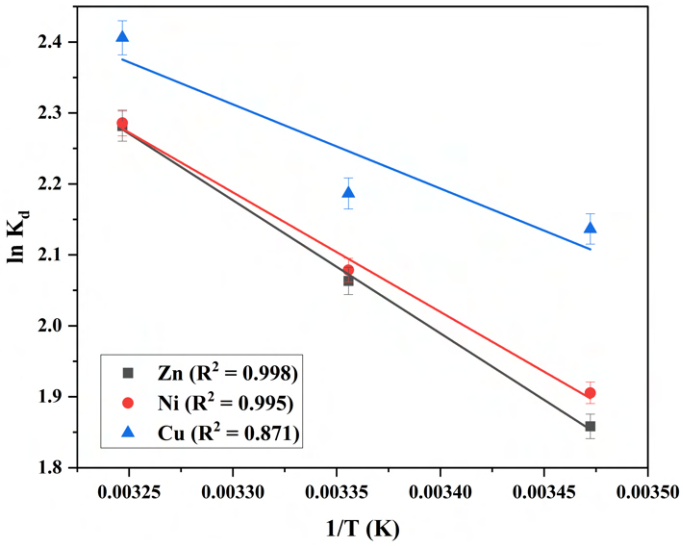

Figure 4.12: Plot of ln K_d vs. 1/T for composite as adsorbent

Table 4.4: Thermodynamic parameters for composite as adsorbent

Temperature (K)		288	298	308
ΔG (J/mol)	Cu^{2+}	-1258.88	-1591.48	-1924.08
	Ni^{2+}	-6781.6	-7363.6	-7945.6
	Zn^{2+}	-5024.88	-5689.98	-6355.08
ΔS (J/mol K)	Cu^{2+}	33.26		
	Ni^{2+}	58.20		
	Zn^{2+}	66.51		
ΔH (J/mol K)	Cu^{2+}	8.32		
	Ni^{2+}	9.98		
	Zn^{2+}	14.13		

posite. The dehydration consumed energy and is preferred at higher temperatures [284], [285]. The positive value of ΔS depicted increased randomness at the solid-aqueous interface [274], [286].

Similar results were found by Shirvani et al., 2015 [284] while investigating the thermodynamics of nickel adsorption on Ca-bentonite. Furthermore, Anirudhan and Suchithra, 2010 [283] studied adsorption of Cu^{2+}, Zn^{2+} and Cd^{2+} on hydrotalcite and discovered that the adsorption occurred spontaneously and that ion exchange was the predominant

adsorption process.

4.2.8 Optimization Study

4.2.8.1 Effect of pH

The effect of pH on adsorption of Cu^{2+}, Zn^{2+} and Ni^{2+} is shown in Figure 4.13. The

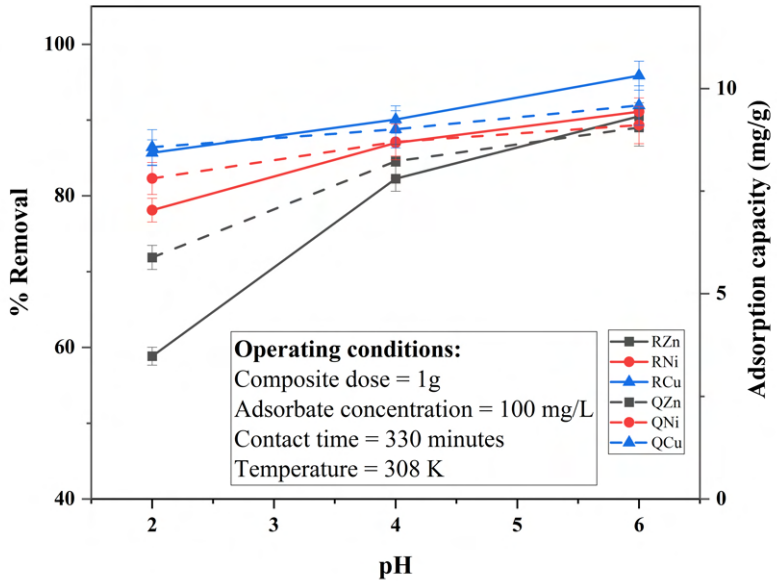

Figure 4.13: Effect of pH on % removal of ternary metal ions and adsorption capacity of composite (-Q is adsorption capacity and -R is % Removal)

percentage adsorption was 85.69%, 78.11%, and 58.84% at pH 2, 90.07, 86.99 and 82.26% at pH 4; and 95.86%, 91.10% and 90.5% at pH 6 for Cu^{2+}, Ni^{2+} and Zn^{2+} ions, respectively. A significant increase in the uptake of Cu^{2+} ions and a modest surge in the uptake of Ni^{2+} and Zn^{2+} ions is observed as the pH increases. At low pH values, the hydrogen ions compete with the metal cation for the same active site and the minimal sorption at pH 2 may be attributed to the high concentration and mobility of H^+ ions in the liquid phase. The decrease in the percentage removal of metal ions at higher concentration of hydrogen ions indicated that the metal ion adsorption was mediated by ion-exchange mechanism. It was mentioned that hydrolysis products and solubility constants (-log K_1) of the metal cations must be considered in the experiments of the pH optimization [287]. Copper is adsorbed as Cu^{2+}, $Cu(OH)^+$, and $Cu_2(OH)_2^{2+}$ when the pH is approximately 6 [288]. In the present work, the pH was limited to values ≤ 6. Above pH 6, metals form insoluble

hydroxide which results in precipitation rather than adsorption [289], [290]. A similar observation was obtained by Aslan et al., 2018 [291] for Cu^{2+} and Ni^{2+} during adsorption study using waste activated sludge.

4.2.8.2 Effect of Composite Dose

Figure 4.14 shows effect of the composite dose on the percentage removal of ternary metal ions and composite adsorption capacity. An increase in the composite dose from 1 to 2 g resulted in enhanced percentage removal of Cu^{2+}, Ni^{2+} and Zn^{2+} ions. The amount of metal ions adsorbed increases from 94.74% to 98.75% for Cu^{2+}, 90.68% to 95.65% for Ni^{2+} and 88.7% to 93.9% for Zn^{2+}. The boosted percentage removal of Cu^{2+}, Ni^{2+} and Zn^{2+} was due to increased surface area and number of active sites available on the composite. However, adsorption capacity demonstrated an opposite pattern to percentage removal. Adsorption capacity of composite decreased from 9.47 to 4.94 mg/g for Cu^{2+}, 9.06 to 4.78 mg/g for Ni^{2+} and 8.87 to 4.69 mg/g for Zn^{2+}, respectively. This decrease was attributed to the overlapping or grouping of active sites which increases the diffusion path length for metal ions to the composite surface.

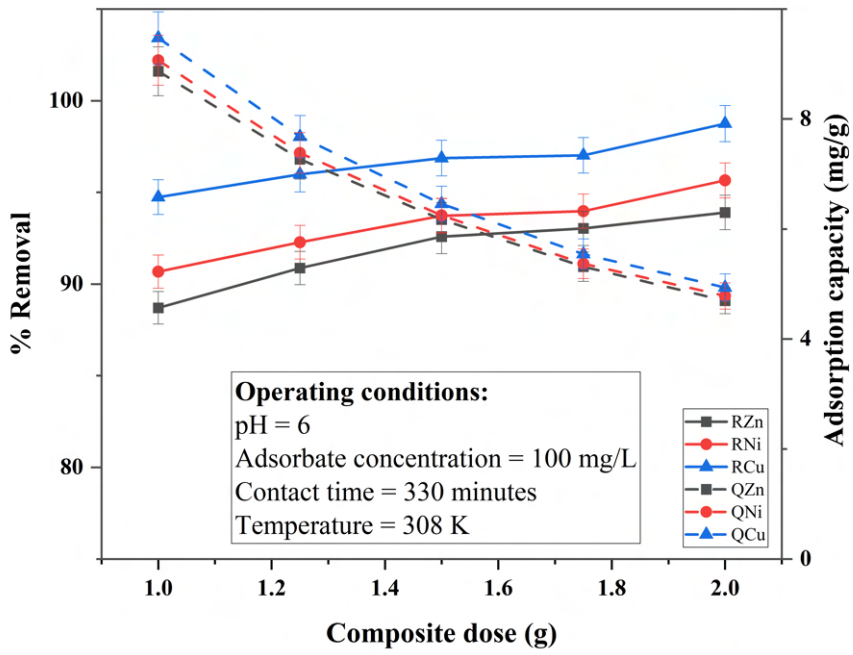

Figure 4.14: Effect of composite dose on % removal of ternary metal ions and adsorption capacity of composite

The similar trend in adsorption capacity was observed in the study of Yildiz et al., 2017 [292] during removal of $Cu^{2+}$and Ni^{2+} ions from synthetic water using tobacco stalks. Aggregation rose continuously with the simultaneous surge in weight of the composite. Also, the higher composite dose lead to a greater number of unsaturated active sites. Consequently, the amount of metal ions adsorbed per unit of composite mass was reduced after increasing the composite dose, which led to decrement in q_e. Esmaeili et al., 2019 [293] observed that the uptake capacity followed the order: bentonite clay > red earth > volcanic ash in adsorption of Cu^{2+}, Ni^{2+} and Zn^{2+}, which displayed that bentonite clay and red earth have the tremendous capacity to adsorb heavy metals. Liu and Zhou, 2010 [224] also mentioned that Cu^{2+} adsorption was higher than Ni^{2+}, similar to the present study.

4.2.8.3 Effect of Initial Concentration

The effect of the initial concentration of ternary metal ions is shown in Figure 4.15. It is

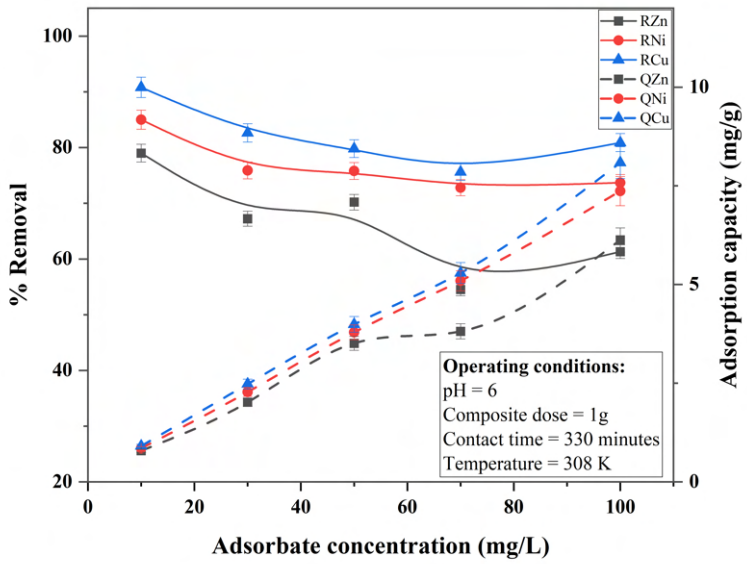

Figure 4.15: Effect of initial concentration of ternary metal ions on % removal and adsorption capacity of composite

evident from Figure 4.15 that percentage removal decreased from 90.8% to 80.88%, 85% to 73.68% and 79% to 61.3% for Cu^{2+}, Ni^{2+} and Zn^{2+} ions, respectively as the metal's concentration increased from 10 to 100 mg/L. Such a reduction was attributed to a fixed number of active sites in the composite, and all active sites are completely occupied at

higher metal concentrations. Similar result was observed during adsorption of Cu^{2+} ions on montmorillonite clay [294].

The adsorption capacity of composite augmented with an increase in the metal ion concentration. This increase was attributed to increased concentration gradient, a driving force for overcoming the mass transfer resistance between metal ions and the solid phase.

4.2.8.4 Effect of Contact Time

The effect of contact time on adsorption of ternary metal ions is shown in Figure 4.16. The adsorption of ternary metal ions on composite increased with escalation of contact time up to 270 minutes for $Cu^{2+}$and Ni^{2+}ions and 330 minutes for Zn^{2+} ions.

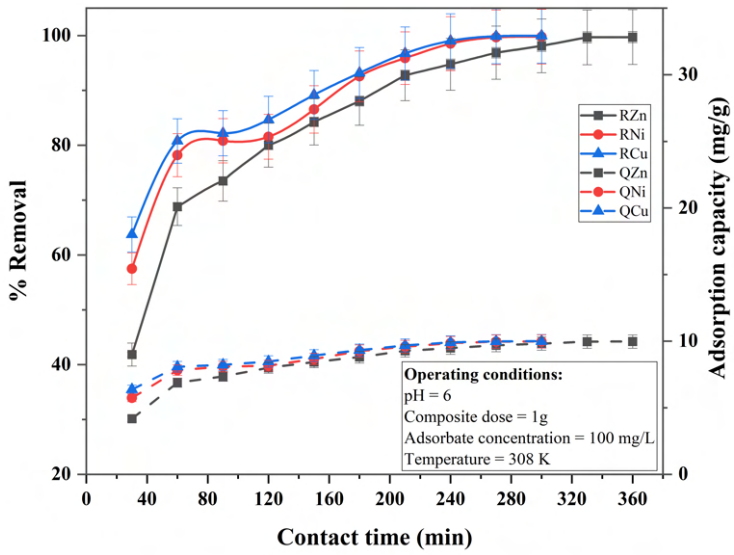

Figure 4.16: Effect of contact time on % removal of ternary metal ions and adsorption capacity of composite

Thereafter, there were no significant increase in the removal of these metal ions. Significant removal of ternary metal ions occurred in mentioned time and the order of adsorption of metal ions was $Cu^{2+} > Ni^{2+} > Zn^{2+}$. These results were similar to the results of Liu and Zhou, 2010 [224]. The disparity in chemical affinity and composite ion exchange ability for the specific chemical group led to variations in the removal of Cu^{2+}, Ni^{2+} and Zn^{2+} ions under similar experimental conditions. Furthermore, researchers [295], [296] observed 2 hours equilibrium contact time during adsorption of Cu^{2+}, Ni^{2+} and Zn^{2+} ions

on fly ash and feat.

4.2.8.5 Effect of Temperature

The temperature effect on adsorption of ternary metal ions is shown in Figure 4.17.
It is evident from Figure 4.17 demonstrated the adsorption of metal ions became more effective as the temperature was increased from 288 K to 308 K. This showed that the adsorption of Cu^{2+}, Ni^{2+} and Zn^{2+} was endothermic.

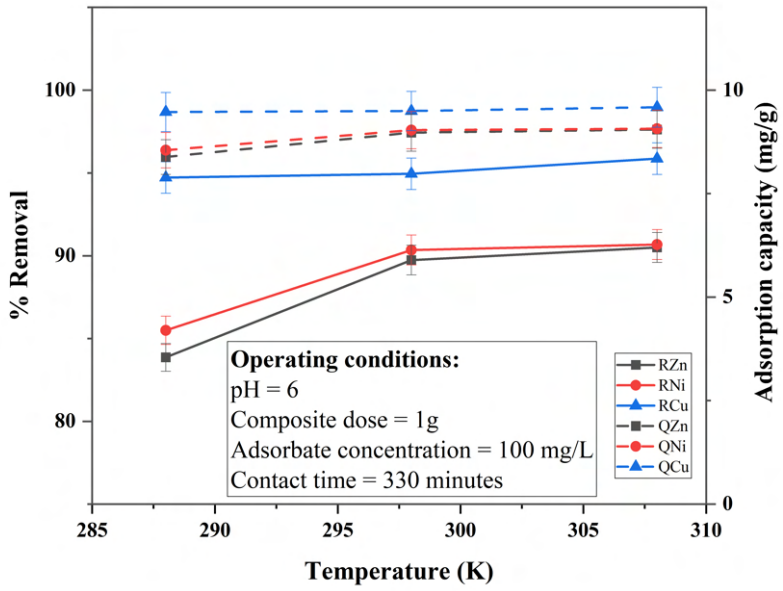

Figure 4.17: Effect of temperature on % removal of ternary metal ions and adsorption capacity of composite

Increased adsorption at higher temperature was attributed to generation of more active surface sites on the composite and reduced boundary thickness around the composite which reduced the mass transfer resistance in the boundary layer [297]. A research study [298] conveyed that adsorption of Cu^{2+} and Zn^{2+} onto natural clay at 25°C, 30°C and 35°C showed endothermic tendency.

4.3 Adsorption Mechanism for composite

The study of pH showed that electrostatic attraction between M^{2+} (M is Cu, Ni and Zn) ions and negatively charged composite surfaces were involved in adsorption [299]. Also,

both cation exchange in the interlayers between permanent negative charge and ternary metal ions and the generation of inner-sphere complexes through the presence of Si–O^- and Al–O^- groups at the composite edges can be used to adsorb ternary metal ions [300], [301]. Metal ion exchange occurs via isomorphous substitution, broken bonds and replacement in composites. The most prevalent isomorphous substitutions in bentonite are Mg^{2+} for Al^{3+} in the octahedral sheets and Al^{3+} for Si^{4+} in the silica sheet. This is where most of the composite exchange capacity comes from. Only 20% of the total exchange capacity is provided by exchange sites along particle edges and on non-cleavage surfaces in broken bonds. A broken bond site's prominence decreases as particle size increases and in replacement; the hydrogen of an exposed hydroxyl is replaced by metal cations.

In the adsorption, Al^{3+}, Ca^{2+} and Mg^{2+} of composite can be exchanged for M^{2+} in solution via cation exchanges. Consequently, possible M^{2+} adsorption mechanisms on composites can be demonstrated by Eqs. 4.1, 4.2 and 4.3 [302], [303]. The adsorbed amount of the M^{2+} from aqueous phase have been tested by adsorption isotherm analysis in order to further validate the potential adsorption mechanism.

$$(Composite) - Ca^{2+} + M^{2+} \rightarrow (Composite) - M^{2+} + Ca^{2+} \tag{4.1}$$

$$(Composite) - COO^- + M^{2+} \rightarrow (Composite - COO^-)_2 M \tag{4.2}$$

$$2(Composite) - OH + M^{2+} \rightarrow (\equiv Composite - O)_2\, M + 2H^+ \tag{4.3}$$

Additionally, FTIR analysis of composite was used to determine the active functional groups involved in complexation reactions (Figure 4.4). Before and after the ternary metal ions adsorption, there were displacements in the composite. Firstly, the intensity of almost all of the infrared bands appeared to decline, and the decreasing vibration intensity indicated that such material had undergone chemical changes [304]. There were evident displacements at 3444.32 and 3430.37 cm^{-1} and 1034.47 cm^{-1} to 1027.90 cm^{-1} showed adsorption involves OH and Si-O stretching.

Thus, ion exchange and surface complexation are the main mechanism responsible for

adsorption of M^{2+} on composite.

4.4 Comparative Study

The adsorption capacity of composite is compared with other adsorbents in Table 4.5. Though the uptake capacities cited in Table 4.5 are derived in different experimental conditions yet it provides significant information of adsorbent selection for continuous reactor system. It is apparent from Table 4.5 that the uptake capacity of the composite developed in the present work is relatively higher after adding red mud [305] with bentonite clay and far more pragmatic than the other inorganic adsorbents developed in other researches.

Table 4.5: Comparison of adsorption capacities of inorganic adsorbents and composite synthesized in the present work

Adsorbent	**Uptake capacity (mg/g)**			**References**
	Cu^{2+}	**Ni^{2+}**	**Zn^{2+}**	
Modified clay sorbent	80.3	23.3	26.6	[289]
Raw calcareous clay	370.37	-	38.17	[281]
Smectite clay	172.41	-	102.04	[281]
Treated calcareous clay	140.84	-	49.75	[281]
Nano structures kaolinite	45.87	-	52.63	[306]
Kaolinite	-	1.67	10.79	[307]
Bentonite	-	33.12	40.34	[308]
Nano kaolinite	125	111	100	[309]
Natural clay	44.84	-	80.64	[310]
Brazilian bentonite clay	11.89	-	-	[311]
Nanoscale zero-valent iron impregnated with clays	5.5	2.1	21.8	[312]
Raw Algerian Bentonite clay	58.82	6.56	19.53	[313]
Bentonite clay and red ochre composite	61.86	37.89	10.48	**Present study** [314]

4.5 Conclusion

The ultimate analysis of the composite confirmed the presence of C, H, and N. These elements were the major component that are helpful in the adsorption of metal ions. The pH value of 6 was found to be optimal, initial concentration of 100 mg/L, contact time of 270 minutes for $Cu^{2+}$and Ni^{2+}ions and 330 minutes for Zn^{2+} ions, temperature of 308 K, and composite dose of 1 g. A correlation plot of experimental and ANN predicted values showed a high correlation coefficient of 0.99 which implied that the chosen trained network was appropriate in predicting output function. Dimensionless numbers φ (63.77, 52.61 and 19.46), N_k (28.20, 34.18 and 92.40) and λ (4.72×10^{-4}, 1.69×10^{-3} and 3.74×10^{-3}) for Cu^{2+}, Ni^{2+} and Zn^{2+} ions, respectively showed that adsorption on the surface of composite was diffusion controlled for Cu^{2+}, Ni^{2+} and mixed diffusion and transfer controlled for Zn^{2+} ions. The adsorption of ternary metal ions on the surface of composite indicated better goodness of fit of Langmuir isotherm (SSR = 2.60, 37.88 and 1.63 for Cu^{2+}, Ni^{2+} and Zn^{2+} ions, respectively) together with PSO model (chemisorption mode). The adsorption was endothermic (ΔH = 9862.48, 14009.83 and 15596.15 kJ/mole for Cu^{2+}, Ni^{2+} and Zn^{2+} ions, respectively) and spontaneous with increased randomness at the solid-aqueous interface. A Comparison among adsorption capacities of various inorganic adsorbents with composite proved it as an effective and potent Cu^{2+}, Ni^{2+} and Zn^{2+} ion scavenger. In the end, the concentration of metal ions in residual solution below the permissible limit was achieved in the present work. As a result, the composite developed can be of enormous industrial relevance.